Am J Physiol Renal Physiol 293: F1657–F1665, 2007.
First published September 5, 2007; doi:10.1152/ajprenal.00274.2007.

Interference with TGF-β signaling by Smad3-knockout in mice limits diabetic glomerulosclerosis without affecting albuminuria

Amy Wang,[1] Fuad N. Ziyadeh,[2] Eun Young Lee,[1,3] Petr E. Pyagay,[1] Sun Hee Sung,[4] Steven A. Sheardown,[5] Nicholas J. Laping,[5] and Sheldon Chen[1]

[1]*Division of Nephrology/Hypertension, Northwestern University, Chicago, Illinois;* [2]*Faculty of Medicine, American University of Beirut, Beirut, Lebanon;* [3]*SoonChunHyang University College of Medicine, Cheonan, Korea;* [4]*Department of Pathology, Ewha Womans University, Mok Dong Hospital, Seoul, Korea;* [5]*Urogenital Biology, Cardiovascular Urogenital Centers of Excellence in Drug Discovery, GlaxoSmithKline Pharmaceuticals, King of Prussia, Pennsylvania*

Submitted 14 June 2007; accepted in final form 29 August 2007

Wang A, Ziyadeh FN, Lee EY, Pyagay PE, Sung SH, Sheardown SA, Laping NJ, Chen S. Interference with TGF-β signaling by Smad3-knockout in mice limits diabetic glomerulosclerosis without affecting albuminuria. *Am J Physiol Renal Physiol* 293: F1657–F1665, 2007. First published September 5, 2007; doi:10.1152/ajprenal.00274.2007.—Transforming growth factor (TGF)-β plays a critical role in diabetic nephropathy. To isolate the contribution of one of the signaling pathways of TGF-β, the Smad3 gene in the mouse was knocked out at *exons 2* and *3*, and the effect was studied in streptozotocin (STZ)-induced diabetes over a period of 6 wk. TGF-β activity was increased in the diabetic mice but was not able to signal via Smad3 in the knockout (KO) mice. As expected in the wild type, the kidneys of the STZ-diabetic mice showed both structural and functional defects that are characteristic of diabetic renal involvement. In the Smad3-KO mice, however, the defects that were improved were renal hypertrophy, mesangial matrix expansion, fibronectin overproduction, glomerular basement membrane thickening, plasma creatinine, and the blood urea nitrogen. The parameters not significantly altered by the Smad3-KO were albuminuria, reduction in podocyte slit pore density, and the increase in vascular endothelial growth factor abundance and activity. It seems that the absence of Smad3 modifies the natural course of murine diabetic nephropathy, providing renal functional protection and preventing structural lesions relating to kidney hypertrophy and matrix accumulation, even though albuminuria and changes in podocyte morphology persist. In conclusion, the effects of the Smad3-KO mirror the effects of anti-TGF-β therapy in diabetes, suggesting that the chief component of TGF-β signaling that is relevant to kidney disease is the Smad3 pathway.

streptozotocin; glomerular basement membrane thickening; mesangial matrix expansion; vascular endothelial growth factor; podocyte slit pore density

THE ACCUMULATION OF EXTRACELLULAR matrix proteins in the glomerular and tubulointerstitial spaces is a hallmark of diabetic kidney disease. The resulting diabetic glomerulosclerosis and tubulointerstitial fibrosis are thought to directly compromise filtration and nephron function, thus leading to progressive renal insufficiency. The matrix accumulation, to a large extent, is incited by the profibrotic cytokine, transforming growth factor-β (TGF-β). Specific inhibition of TGF-β activity by a neutralizing antibody or other means successfully prevents mesangial glomerulosclerosis, extracellular matrix overexpression, renal hypertrophy, and renal insufficiency in animal models of diabetic nephropathy (3, 11, 17, 23). However, the exact intracellular signaling mechanisms in the TGF-β pathway that are responsible for diabetic nephropathy remain to be defined.

Basic research on the action of TGF-β has uncovered a multitude of downstream signaling pathways and cross talk, but predominant among them is the intracellular Smad pathway. The Smad family comprises several members, but Smad2 and Smad3 in particular are governed by the TGF-β ligand. After activation by phosphorylation and partnering with a co-Smad4, the R-Smads translocate into the nucleus and, in conjunction with other transcription factors, help direct the activation and repression of genes regulated by TGF-β (2). Smad3 is thought to be the signaling arm that primarily mediates the autoinduction of TGF-β and its effects on apoptosis and matrix expression (1, 7, 15, 16, 21). Smad2 overlaps somewhat with Smad3 (and also has its own distinctive effects) (13), but overall Smad2 seems to be relatively less important in the kidney, perhaps owing to its lack of sequence-specific DNA binding activity (18).

Given the centrality of the TGF-β system in the pathogenesis of diabetic nephropathy, we investigated the role of Smad3 in mediating the adverse effects of diabetes on the kidney. The mouse Smad3 gene was knocked out at *exons 2* and *3*, and in the process a nonsense mutation was introduced in *exon 4* that truncates the Smad3 protein at 77 amino acids (out of a normal 425 amino acids). Type 1 diabetes, induced by injections of streptozotocin (STZ), was sustained for 6 wk, at which time albuminuria was a prominent feature, and the mice were analyzed for the effect of the Smad3 knockout (KO) on diabetic renal manifestations. We focused on hypertrophy and matrix-related changes, such as glomerular basement membrane (GBM) thickening, mesangial matrix expansion, and fibronectin production. Also examined were functional measures, including blood urea nitrogen (BUN), plasma creatinine, albuminuria, vascular endothelial growth factor (VEGF) expression and signaling, and podocyte morphometry.

MATERIALS AND METHODS

Smad3-KO mouse. All protocols using rodents were approved by the Institutional Animal Care and Use Committee and were in compliance with the *NIH Guide for the Care and Use of Laboratory Animals*. The homology arms that flank *exons 2* and *3* of Smad3 were subcloned from a bacterial artificial chromosome, derived from a 129/Sv

Address for reprint requests and other correspondence: S. Chen, Northwestern Univ., 303 E. Chicago Ave., Tarry 4-755, Chicago, IL 60611 (e-mail: sheldon-chen@northwestern.edu).

The costs of publication of this article were defrayed in part by the payment of page charges. The article must therefore be hereby marked "*advertisement*" in accordance with 18 U.S.C. Section 1734 solely to indicate this fact.

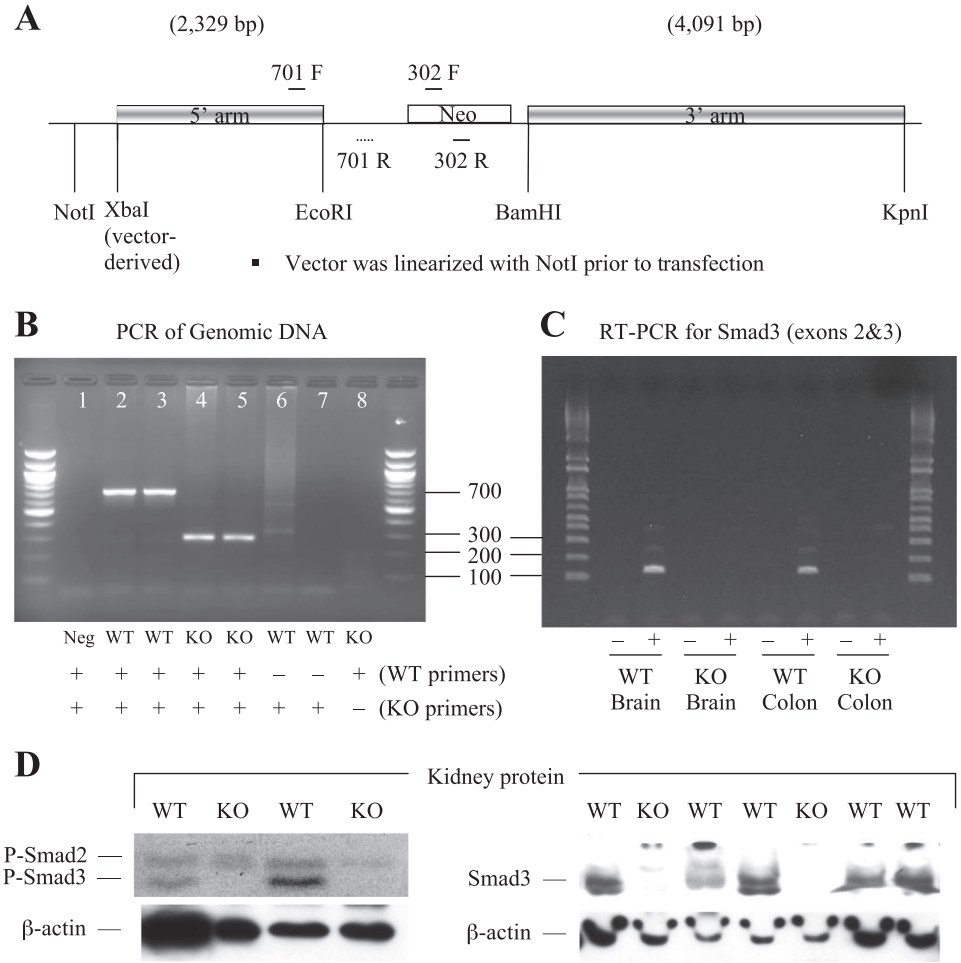

Fig. 1. *A*: schematic of the targeting vector to knock out (KO) *exons 2* and *3* of the mouse Smad3 gene. The 5′ and 3′ homology arms were cloned into a vector with a neomycin (Neo) resistance cassette. Also depicted are the positions of the genotyping primers that distinguish between the wild-type (WT) and KO alleles. The "WT" primers yield a 701-bp PCR product (701 R primer will not bind to the KO allele), whereas the "KO" primers yield a 302-bp product. *B*: PCR done on genomic DNA with all four primers confirms that WT mice contain at least one WT Smad3 allele (701 bp), and KO mice contain only the targeted allele (302 bp, within Neo). Controls included no template (Neg), WT genomic DNA attempted with "KO" primers (*lanes 6* and *7*), and KO DNA attempted with "WT" primers (*lane 8*). The WT and KO mice shown here were representative of the entire group. *C*: RT-PCR done on total RNA from brain and colon confirms the presence of the Smad3 message at *exons 2* and *3* in the WT mice (expected 141-bp product) and the absence of Smad3 mRNA in the KO mice. The negative controls (−) consisted of running the RT-PCR without reverse transcriptase. *D*: absence of phosphorylated and total Smad3 protein in the kidneys of Smad3-KO mice. The Western blot shows that Smad2 is present throughout, but phospho-Smad3 and total Smad3 are absent in the KO mice. The β-actin bands indicate that protein is present in all lanes.

bacterial artificial chromosome library (Research Genetics), into the pMC1Neo plasmid to generate the targeting construct (Fig. 1*A*). The targeting vector was linearized by *Not* I, and 25 μg were electroporated into 2×10^7 embryonic stem (ES) cells (E14.1, from 129/OLA/Hsd strain), using a Bio-Rad Gene Pulser set at 240 V and 500 μF. Selection by G418 (400 μg/ml) was applied on the following day and maintained for an additional 8–10 days until G418-resistant ES colonies were sufficiently large. Successful recombination events that knocked out Smad3 were confirmed by Southern blot, with the probe being a 1.8-kb sequence generated by *Xma* I/*Bgl* II digestion and hybridizing external to the 5′ homology arm. The diagnostic bands resolve as 6.5-kb [wild type (WT)] and 5.5-kb (KO) in length. KO ES clones were injected into host blastocysts using standard procedures, and the resulting chimeric males were mated to C57BL/6 females for germline transmission. The backcross was continued onto the C57BL6/Ola strain for at least six generations.

Treatment protocol. Out of the original 15 male Smad3-KO mice that were age-matched with WT mice and then randomized, 10 mice survived to the end of the experiment: one group that remained nondiabetic ($n = 4$) and another group that received STZ ($n = 6$). As WT controls, 18 male littermate mice were matched for age and assigned to remain nondiabetic ($n = 9$) or to be induced with diabetes via STZ ($n = 9$). STZ dissolved in citrate buffer, pH 5.5, and was given intraperitoneally at 100 mg/kg per day for 3 consecutive days (17). The onset of diabetes was confirmed by the presence of glucosuria on urinary dipstick. The WT and KO mice randomized to remain nondiabetic received only the vehicle, citrate buffer. Additionally for the STZ-diabetic mice, insulin pellets (LinShin) were implanted subcutaneously in the interscapular area. All animals were provided food and water ad libitum. The baseline 18-h urine collection showed that albumin excretion rates (AER) were similar across all groups (data not shown). The experiment was terminated after 6 wk, at which time the mice underwent a final 18-h urine collection. Blood was obtained from the retroorbital sinus during terminal anesthesia with isoflurane. Euthanasia was done by cervical dislocation, and the heart and two kidneys were harvested.

PCR genotyping. Primers were designed to detect the Smad3-WT allele in the area of the 5′ homology arm. WT forward is 5′-TT-

Table 1. *Characteristics of the WT and Smad3-KO mice at death, both nondiabetic and streptozotocin-diabetic*

	n	Body Weight, g	Kidney/Body Weight, mg/g	Heart Weight, g	Plasma Glucose, mg/dl
Nondiabetic WT	9	30.4±0.9	14.2±0.4	0.17±0.01	106±16
Nondiabetic KO	4	28.0±1.0	13.2±0.7	0.18±0.01	96±17
STZ-diabetic WT	9	23.4±1.3*	18.7±0.7*	0.16±0.02	523±39*
STZ-diabetic KO	6	26.8±1.4	13.7±0.8	0.18±0.01	411±39*

Values are means ± SE; *n*, no. of mice. WT, wild type; KO, knockout; STZ, streptozotocin. *$P < 0.01$ vs. nondiabetic WT.

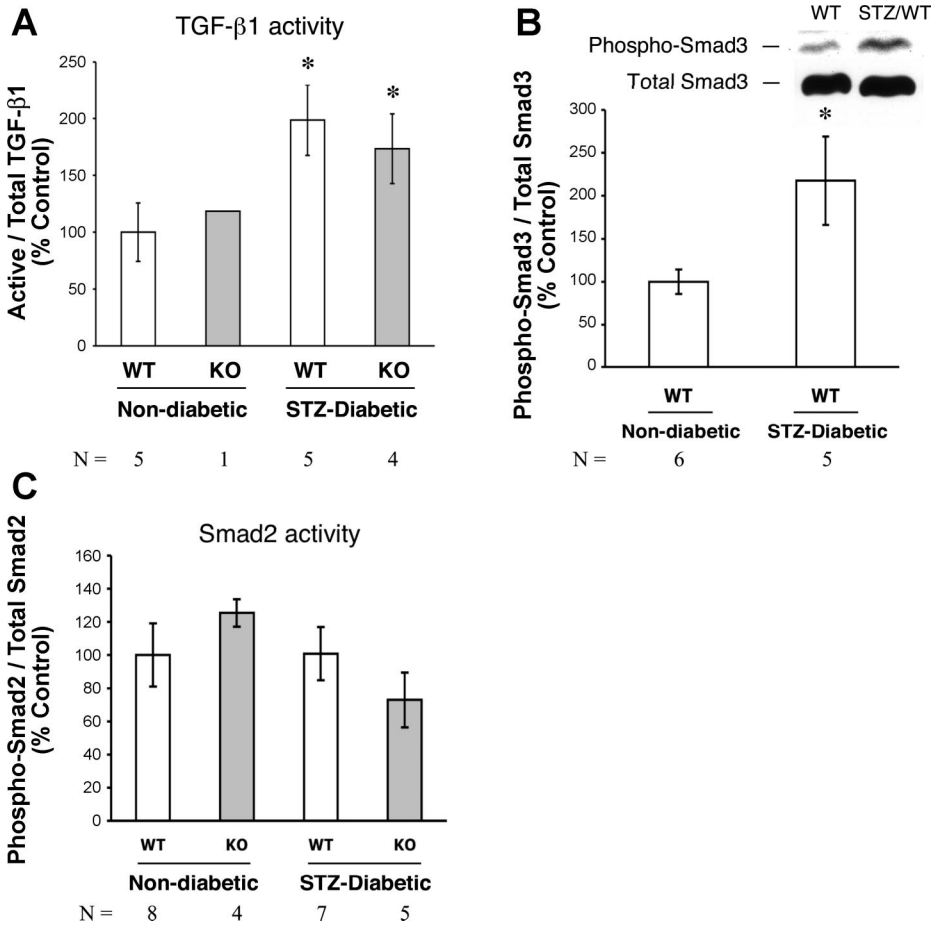

Fig. 2. Transforming growth factor (TGF)-β_1, Smad3, and Smad2 activities. *A*: the ratio of active (free) TGF-β_1 to total TGF-β_1 protein, measured by ELISA, was significantly increased in the kidney lysates of streptozotocin (STZ)-diabetic WT mice (*$P < 0.01$ vs. nondiabetic WT) and remained elevated in the diabetic Smad3-KO (*$P = 0.05$ vs. nondiabetic WT). *B*: downstream of the increased TGF-β_1 activity was a demonstrable increase in the ratio of phosphorylated Smad3 to total Smad3, signifying activation of Smad3 in diabetes (*$P < 0.05$ vs. nondiabetic WT). KO mice were not analyzed because of the absence of Smad3. *C*: analysis of Smad2 activity, by measuring the phospho-Smad2-to-total Smad2 ratio, did not reveal any significant changes because of the Smad3 KO.

GCATAGTCAGGAGCATCTTC-3′; WT reverse is 5′-CAGGGTGGAAGCCAAGTATAAG-3′; and predicted size is 701 bp. The WT primers will not detect a homozygous Smad3-KO genotype, because the WT reverse primer binds to a sequence that does not exist in the KO allele (Fig. 1*A*). To detect the Smad3-KO genotype, primers were designed to amplify the neomycin cassette. KO forward is 5′-AGAGGCTATTCGGCTATGACTG-3′; KO reverse is 5′-AGCCATGATGGATACTTTCTCG-3′; and predicted size is 302 bp. All four primers, WT forward/reverse and KO forward/reverse, were used simultaneously in the PCR genotyping of each Smad3-WT or -KO mouse. PCR denaturation was at 94°C for 2 min, followed by 35 cycles of denaturation at 94°C for 20 s, annealing at 56°C for 20 s, extension at 68°C for 1 min, and ending with extension at 68°C for 7 min. PCR products were analyzed by electrophoresis.

RT-PCR for Smad3. Total RNA was extracted from the brain and colon of Smad3-WT and -KO mice using TRIzol reagent (Invitrogen, Carlsbad, CA). Two micrograms of each RNA sample were reverse-transcribed using SuperScript II (Invitrogen). The resulting cDNA was PCR amplified using the forward primer 5′-GCACAGCCACCATGAAT-3′ (in Smad3 *exon 2*) and the reverse primer 5′-GTGTGGCGTGGCACCAAC-3′ (in *exon 3*). The predicted product size is 141 bp in WT mice, whereas no product is expected in KO mice. PCR denaturation was at 95°C for 5 min, followed by 35 cycles of denaturation at 95°C for 15 s, annealing

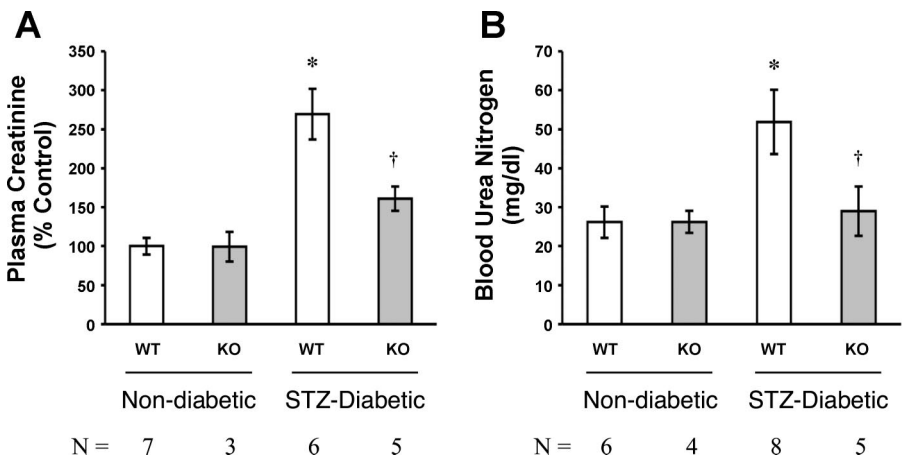

Fig. 3. Renal function. *A*: the mean plasma creatinine, measured by HPLC, was significantly elevated in the diabetic WT mice (*$P < 0.01$ vs. nondiabetic WT), compatible with reduced kidney filtration function. The increase in plasma creatinine with diabetes was prevented in the Smad3-KO mice (†$P < 0.01$ vs. STZ-diabetic WT). *B*: blood urea nitrogen (BUN) tracked with the plasma creatinine, increasing in diabetic WT mice (*$P < 0.05$ vs. nondiabetic WT) but remaining normal in diabetic KO mice (†$P < 0.05$ vs. STZ-diabetic WT).

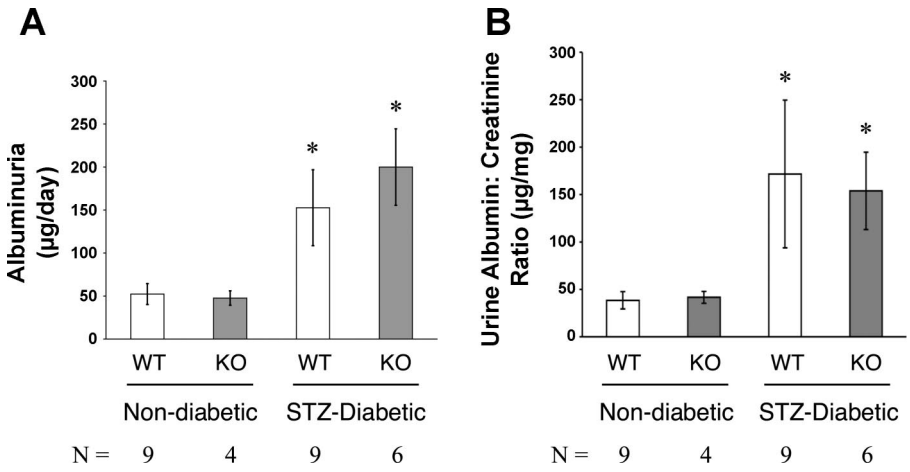

Fig. 4. Albuminuria. *A*: diabetic mice, whether WT or KO, developed albuminuria that was roughly three times greater than in the nondiabetic WT mice (*$P < 0.05$). The KO of Smad3 did not significantly affect the albumin excretion rate (AER) per day (P = not significant for STZ-diabetic KO vs. diabetic WT). *B*: expressing albuminuria as the ratio of albumin to creatinine in a spot urine sample was comparable to the data depicting AER per day (*$P < 0.05$ vs. nondiabetic WT).

at 54°C for 15 s, extension at 72°C for 15 s, and finishing with extension at 72°C for 5 min.

Western blotting. Kidney protein from each mouse was extracted in RIPA lysis buffer using mechanical homogenization techniques. Equalized concentrations of proteins were subjected to sodium dodecyl sulfate-polyacrylamide gel electrophoresis (NuPAGE, Invitrogen) and electrically transferred onto a nitrocellulose membrane, which was probed with primary antibodies against phospho-Smad2/3 (Millipore, Billerica, MA), total Smad2 (Zymed/Invitrogen), total Smad3 (AnaSpec, San Jose, CA), phospho-VEGFR-2 (EMD Biosciences), total VEGFR-2 (Lab Vision), fibronectin (Lab Vision), and β-actin (Sigma, St. Louis, MO). The Western signal was developed with the appropriate horseradish peroxidase-tagged secondary antibody and chemiluminescence substrate (Pierce, Rockford, IL). Densitometry of the bands captured on film was performed with ImageJ software (NIH, Bethesda, MD), corrected for β-actin, and compared with control.

Analytic procedures. Plasma was submitted to Thomas Jefferson University (Philadelphia, PA) for an accurate measurement of creatinine concentration by high-performance liquid chromatography (6). BUN was measured by a colorimetric-based assay kit (BioAssay Systems, Hayward, CA). The plasma concentration of glucose, from a random blood sample obtained at death, was measured by the glucose oxidase method using an automated analyzer, the YSI 2300 STAT Plus (YSI, Yellow Springs, OH). Urinary albumin concentrations were determined by the Albuwell M kit (Exocell, Philadelphia, PA), an indirect ELISA. Urine creatinine concentration was assayed with the Creatinine Companion kit (Exocell). The data were used to calculate the AER per day and the urine albumin-to-creatinine ratio.

ELISA for TGF-β_1. TGF-β_1 in the kidney protein lysates was detected by a commercial ELISA kit (R&D Systems, Minneapolis, MN). Both active (i.e., free) TGF-β_1 and total TGF-β_1 were assayed separately for each kidney sample and read off of a concurrently performed standard curve. The active-to-total TGF-β_1 ratio, indicative of the fraction of total TGF-β_1 that is in the active form, is reported as a percentage of the control (nondiabetic WT group).

Renal morphometrics. For ultrastructural evaluation, kidney tissue was fixed in 3% glutaraldehyde, postfixed in 1% osmium tetroxide, and embedded in epoxy resin (epon). The specimen was thin sectioned, stained with lead citrate/uranyl acetate, and examined under a JEOL transmission electron microscope. Electron micrographs of 5–10 glomeruli per kidney were randomly taken at both ×1,500 and ×30,000 for each mouse. At the lower magnification, mesangial matrix was discernible, and its extent was measured as a percentage of the glomerular tuft area, with the aid of Image-Pro Plus software. At the higher magnification, mean GBM thickness was obtained from measurements at three different sites of cross sectioning, with the aid of Image-Pro Plus. Tangentially sectioned GBMs were excluded from the analysis. The mesangial matrix was also assessed by periodic acid-Schiff staining of kidneys fixed in 10% neutral buffered formalin and embedded in paraffin and sectioned at 5 μm.

Photomicrographs of the GBM were also analyzed for the density of open and "tight" slit pores between the podocyte foot processes, according to published methods (12, 20). The numbers of each type of slit pore were counted and divided by the GBM length (mm) to arrive at the linear density of podocyte slit pores.

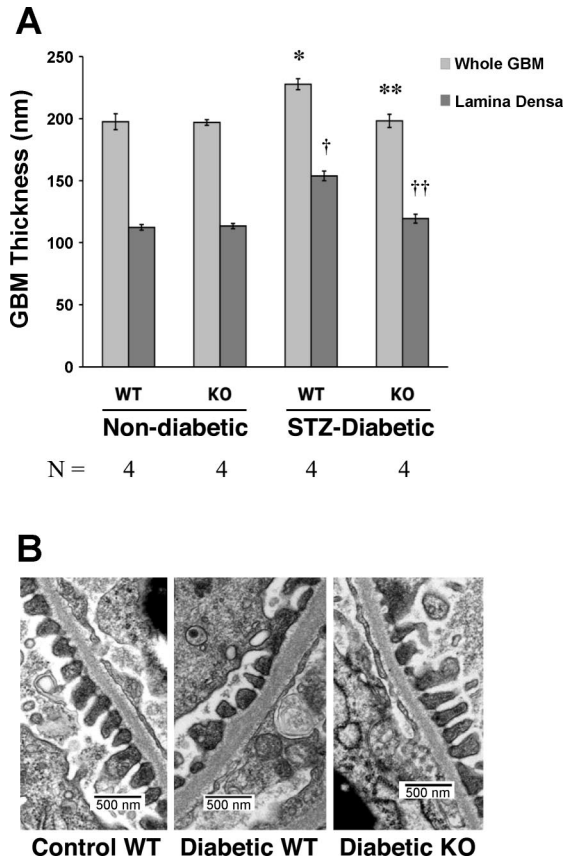

Fig. 5. Glomerular basement membrane (GBM) thickening. *A*: GBM thicknesses were measured across the whole GBM and across the lamina densa. STZ-diabetes caused GBM thickening in the WT mice (* or †$P < 0.01$ vs. nondiabetic WT), but was unable to do so in the Smad3-KO mice (** or ††$P < 0.01$ vs. diabetic WT). *B*: representative electron photomicrographs (magnification: ×30,000) show diabetic GBM thickening and its prevention in the Smad3-KO mice.

Immunohistochemistry. On 4-μm kidney sections, endogenous peroxidases were quenched with 2.25% H_2O_2, and nonspecific binding sites were blocked with avidin/biotin (Vector Laboratory, Burlingame, CA). Primary anti-VEGF antibody was added (1:500 dilution, Lab Vision, Fremont, CA), followed by biotinylated anti-rabbit secondary antibody (1:1,000) and avidin-conjugated horseradish peroxidase. Signal was developed with diaminobenzidine substrate, and the sections were counterstained with Gill's no. 2 hematoxylin. Nonspecific staining was assessed by omitting the primary antibody. Photomicrographs of at least 20 fields in each mouse were quantitated for the intensity of peroxidase staining in the glomeruli with IPLab software (Scanalytics, Fairfax, VA).

Statistical analysis. Table and graphical data are displayed as the mean ± SE for the number of animals indicated. Values for each of the four groups of animals were compared using one-way analysis of variance and the post hoc Tukey's test. When data were relevant for only two of the groups, e.g., Smad3 activation in the WTs, the unpaired Student's *t*-test was used. Statistical significance was set at $P < 0.05$.

RESULTS

Verification of Smad3 KO. Genotyping of the Smad3-WT and -KO mice was done by PCR using primers that are specific for either the WT or KO allele, with predicted product sizes of 701 and 302 bp, respectively. Using the WT ("701") and KO ("302") primer sets simultaneously, PCR revealed a 701-bp band in all of the WT mice. On the other hand, all of the KO mice showed only the 302-bp band, indicating homozygosity for the targeted Smad3-KO allele (Fig. 1*B*). Genomic DNA from homozygous WT mice (*lanes 6* and *7*) could not be amplified with the "KO primers," and genomic DNA from KO mice (*lane 8*) could not be amplified with the "WT primers."

Smad3 gene expression was examined next. Evidence of the mRNA was sought by RT-PCR, specifically looking for *exons 2* and *3*, which were deleted in the KO mice. In total RNA preparations from brain and colon, the expected 141-bp band

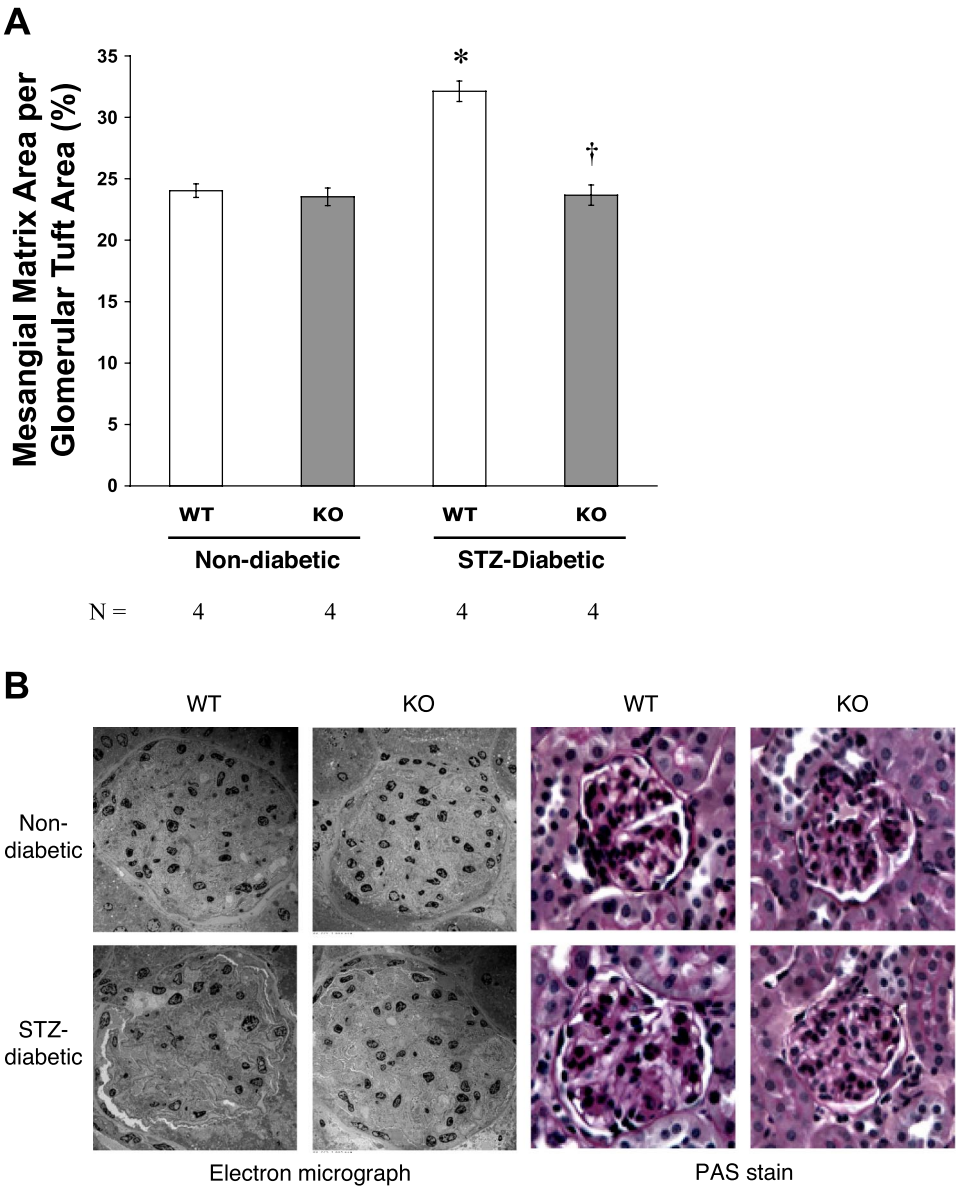

Fig. 6. Mesangial matrix expansion. *A*: as assessed by electron microscopy, the area of the glomerular tuft occupied by mesangial matrix was expressed as a percentage. STZ-diabetes induced mesangial matrix expansion in the WT mice (*$P < 0.01$ vs. nondiabetic WT) but failed to do so in the Smad3-KO mice (†$P < 0.01$ vs. STZ-diabetic WT). *B*: the increased mesangial matrix in representative electron photomicrographs (magnification: ×1,500) and periodic acid-Schiff stains (magnification: ×400) is evident in the diabetic WT mice and ameliorated in the diabetic KO mice.

appeared only in the WT mice and never in the KO mice (Fig. 1*C*).

Finally, Smad3 was assayed at the protein level to provide proof of the KO. By Western, phospho-Smad3 was present in all of the WT mice but none of the KO mice (Fig. 1*D*). Similarly, total Smad3 protein was detectable in WT mice but was completely absent in the KO mice (Fig. 1*D*). Adequate loading of the electrophoresis gel can be seen in the phospho-Smad2 and the β-actin bands.

Characteristics of the mice. At the end of the 6-wk experimental period, the nondiabetic WT and KO mice had similar weights. With poorly controlled STZ-induced diabetes, the WT mice lost significant amounts of weight (Table 1). In terms of total kidney mass corrected for body weight, WT mice showed a significant increase with diabetes, whereas the Smad3-KO mice showed no such increase in renal mass. Heart weights did not differ between any of the groups (P = not significant). Finally, plasma glucose concentrations were elevated in both STZ-diabetic groups, and the degree of hyperglycemia was not significantly different between WT and KO mice (523 vs. 411 mg/dl, respectively, P = not significant).

Renal TGF-β_1, Smad3, and Smad2 activities. The activity of TGF-β_1 was measured as the ratio of free (active) TGF-β_1 to total TGF-β_1 in preparations of kidney cortex protein lysates. TGF-β_1 activity was increased in the diabetic state, regardless of the Smad3 genotype (Fig. 2*A*). As a result of the increased TGF-β_1 activity, the phosphorylation of Smad3 as a fraction of total Smad3 was increased in the STZ-diabetic WT kidneys (Fig. 2*B*). Smad3 activation could not be assessed in the KO mice. In contradistinction to Smad3, Smad2 activity as evaluated by the ratio of phospho-Smad2 to total Smad2 was unchanged in the kidney of a Smad3-KO (Fig. 2*C*), arguing against a compensatory increase of Smad2 activity as a result of the Smad3 KO.

Renal function. The mean plasma creatinine concentration (Fig. 3*A*) and the BUN level (Fig. 3*B*) were both significantly increased in the STZ-diabetic WT mice vs. nondiabetic WT control. The rise in plasma creatinine with diabetes, however, was largely prevented in the diabetic Smad3-KO mice ($P < 0.01$ vs. STZ-diabetic WT), as was the rise in BUN ($P < 0.05$ vs. STZ-diabetic WT).

Diabetic albuminuria. The mean AER of the diabetic WT mice was roughly triple that of the nondiabetic mice ($P < 0.05$, Fig. 4*A*), but the diabetic albuminuria was not influenced by the Smad3 KO. In the absence of diabetes, the Smad3-KO mice did not spontaneously develop albuminuria. Quantifying albuminuria as the ratio of albumin-to-creatinine in a spot urine sample resulted in a graph (Fig. 4*B*) similar to the one depicting AER per day.

GBM thickening. The GBM thickness was increased by the diabetic state (Fig. 5). In the STZ-diabetic group, however, the Smad3-null genotype resulted in the prevention of GBM thickening. The Smad3-KO mice that remained nondiabetic did not show any change in GBM thickness compared with the control WT mice. Representative electron photomicrographs of the GBM thickness are shown in the control, diabetic WT, and diabetic Smad3-KO mice (Fig. 5*B*).

Mesangial matrix expansion. Expansion of the mesangium with extracellular matrix was quantified by electron microscopy. The mesangial matrix area as a percentage of the glomerular tuft area was enlarged in the STZ-diabetic state (Fig. 6*A*). However, mesangial matrix expansion was completely abrogated in the Smad3-KO mice, evident in the electron photomicrographs and periodic acid-Schiff stains of representative glomeruli (Fig. 6*B*).

Fibronectin expression. The kidney fibronectin content was evaluated by Western blot and found to be increased in the diabetic WT mice compared with nondiabetic controls ($P < 0.01$, Fig. 7). The increase in renal fibronectin with diabetes was significantly diminished by the Smad3 KO. However, for reasons unknown, the control Smad3-KO mice also had increased fibronectin, despite being nondiabetic.

VEGF levels and activity. STZ-induced diabetes significantly increased the level of VEGF protein, quantified by immunohistochemistry, in the periphery and the mesangium of the glomerulus (Fig. 8, *A* and *B*). In nondiabetic animals, the glomerular tuft rims also showed staining for VEGF, compatible with constitutive VEGF expression in the podocytes (19). The Smad3 KO did not influence the ambient level of VEGF in either control or diabetic mice.

VEGF signaling activity was concordant with the VEGF protein levels described above. Measured as the ratio of autophosphorylated VEGFR-2 to total VEGFR-2 (i.e., the extent of VEGFR-2 activation), VEGF activity was increased in the kidneys of both STZ-diabetic groups, irrespective of the Smad3 genotype (Fig. 8*C*).

Slit pore density. The number of slit pores between podocyte foot processes per unit length of GBM, or slit pore density, was significantly decreased in the STZ-diabetic mice (Fig. 9). Concomitantly, the density of "tight" pores, identified as an obliteration of the space between adjacent foot processes, was increased in the STZ-diabetic mice. The KO of Smad3 did not

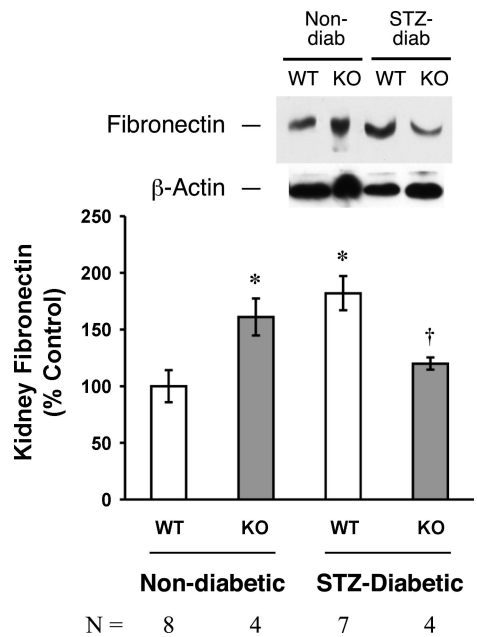

Fig. 7. Kidney fibronectin content. The amount of fibronectin, corrected for β-actin, was increased in the kidneys of STZ-diabetic mice and nondiabetic Smad3-KO mice (*$P < 0.01$ vs. nondiabetic WT). The renal fibronectin buildup in diabetes was prevented by the Smad3-KO (†$P < 0.05$ vs. diabetic WT). A representative Western blot of fibronectin bands, along with the β-actin loading controls, is shown for the four experimental groups of mice.

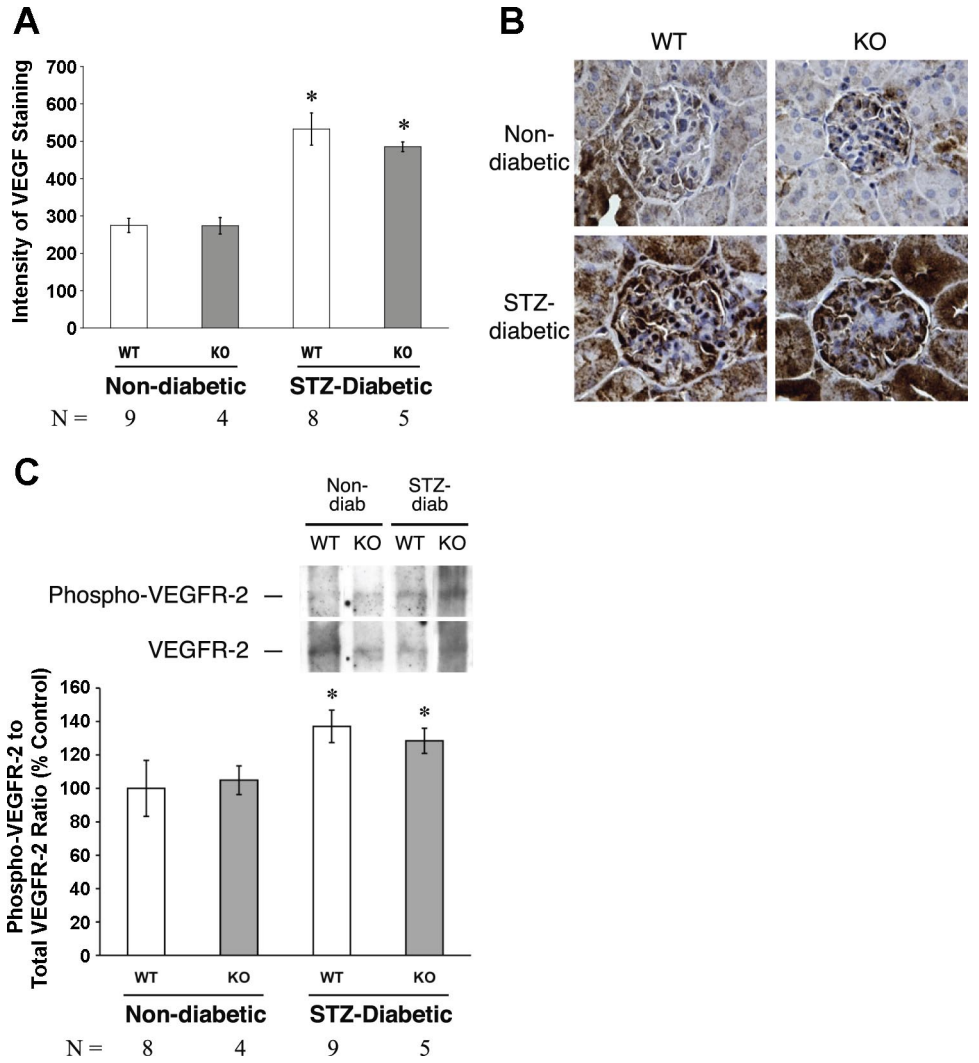

Fig. 8. *A*: glomerular VEGF protein by immunohistochemistry. The intensity of VEGF staining (brown) was increased in the STZ-diabetic state (*$P < 0.01$ vs. nondiabetic WT) but not significantly reduced by a Smad3 KO (P = nonsignificant vs. diabetic WT). *B*: the VEGF increase with STZ-diabetes and the lack of effect with a Smad3 KO are evident in the representative photomicrographs (magnification: ×600). The omission of 1° anti-VEGF antibody was taken to be the background level of peroxidase staining. *C*: VEGF receptor activation in diabetes. The ratio of phosphorylated VEGFR-2 to total VEGFR-2, one indicator of VEGF signaling activity, was increased in STZ-diabetes, regardless of the Smad3 genotype (*$P < 0.05$ vs. nondiabetic WT). Representative Western blots of phospho-VEGFR-2 and total VEGFR-2 are shown (bands juxtaposed from the same chemiluminescence film).

affect the slit pore density in either the nondiabetic or STZ-diabetic states. Changes in the open slit pore and "tight" pore densities were reciprocal to each other.

DISCUSSION

The two sets of diabetic mice, WT and KO, had equal opportunity to develop nephropathy in that both were hyperglycemic and had increased renal TGF-β. The critical difference was that the diabetes-induced increase in TGF-β could not translate into Smad3 activation in the KO mice, resulting in the prevention of TGF-β-related effects that can be categorized along the lines of hypertrophy and fibrosis. How did the diabetic Smad3-KO mice in the present study compare with the diabetic anti-TGF-β-treated mice from a prior study (23)? For the most part, they were concordant in terms of the diabetic kidney lesions that were ameliorated: renal hypertrophy, GBM thickening (4), mesangial matrix expansion, and fibronectin overexpression (23). The prevention of fibronectin overexpression may have its basis in the fact that the fibronectin promoter contains Smad binding elements and the TGF-β-induced gene transcription of fibronectin is Smad3 dependent, as shown by the use of a Smad3 dominant negative (10).

However, the interruption of Smad3 signaling did not improve all aspects of diabetic nephropathy. Albuminuria was not ameliorated by the Smad3 KO, at least not after 6 wk of STZ-induced diabetes. This is not to say that the lack of Smad3 would not have decreased diabetic albuminuria at some point, but ours was not a longitudinal study. Interestingly, albuminuria also failed to improve in the diabetic *db*/*db* mice treated with an anti-TGF-β antibody (2G7) (23), concordant with our Smad3-KO findings. On the other hand, another pan-selective anti-TGF-β antibody (1D11) did reduce proteinuria, albeit in the STZ-diabetic rat after uninephrectomy (3). The intriguing finding from that study was that a different antibody targeting only TGF-β_1 and -β_2 (CAT-192) did not protect against the development of diabetic proteinuria, suggesting that its pathogenesis is influenced principally by the TGF-β_3 isoform (3).

Further complicating the picture is the finding by Fujimoto et al. that diabetic albuminuria is relatively prevented in a different Smad3-KO mouse model (9). At 4 wk of STZ-diabetes, their WT mice (also C57BL/6 strain) showed a urine albumin excretion that was >20-fold increased compared with that of the nondiabetic WT. Compared with the same control,

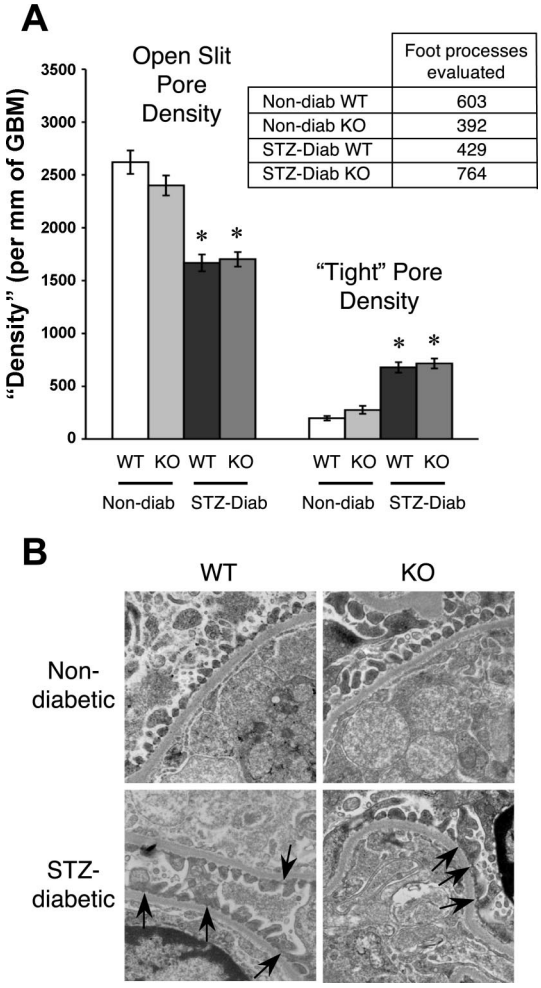

Fig. 9. Podocyte slit pore density. *A*: as assessed by electron microscopy, the number of open slit pores between podocyte foot processes and the number of "tight" pores were expressed per millimeter length of GBM to arrive at the mean numerical "density" (±SE) for each of the four groups of mice. Diabetic WT mice had decreased slit pore density and increased "tight" pore density (*$P < 0.01$ vs. nondiabetic WT). These diabetic changes were not prevented by the KO of Smad3 and were associated with the persistence of albuminuria. *B*: representative electron photomicrographs (magnification: ×30,000) show examples of "tight" slit pores (arrows), which are more prevalent in the STZ-diabetic mice, whether WT or Smad3-KO.

their diabetic KO mice had albuminuria that was "only" fourfold increased. Comparing a >20-fold to a fourfold increase, it may be construed that the Smad3 KO had ameliorated albuminuria. But a fourfold increase is still quite large, and Fujimoto's paper does not reveal whether the difference reached statistical significance, leaving open the interpretation that albuminuria may not have been ameliorated in the diabetic KO when judged against the nondiabetic WT control.

There are key differences in the ways that the Smad3 gene was knocked out in our respective mouse models. Fujimoto's mice lacked *exon 8* (out of 9 exons), and, in splicing *exon 7* to *exon 9*, the Smad3 protein was foreshortened at 340 amino acids, because of a new stop codon in *exon 9* (9, 22). Our KO mice lacked *exons 2* and *3*, which introduces a stop codon in *exon 4*, truncating the Smad3 protein at 77 amino acids. Both Smad3 mutants should be nonfunctional (22), demonstrated by the complete absence of phospho-Smad3. Besides, our 77-amino acid fragment contains just one of the eight phosphorylatable serine/threonine residues (T8). But the Smad3 *exon 8* deletion used by Fujimoto et al. (9) contains five of the eight phosphosites (T8, T179, S204, S208, S213). It remains to be determined whether the molecular and phenotypic differences between our models might explain the disparity in the effect on diabetic albuminuria.

We found support for the persistence of diabetic albuminuria in the Smad3-KO mice by examining the mechanisms related to podocytopathy and a vascular permeability factor, better known as VEGF. The protein levels of VEGF and its signaling via the VEGFR-2 receptor were increased by diabetes and remained elevated in the Smad3-KO group. As a cytokine, VEGF seems to impact the development of diabetic albuminuria more than TGF-β (20, 23), although TGF-β signaling through Smad3 does not appear to be a major determinant of the VEGF increase in the diabetic kidney. In addition, albuminuria correlates with podocyte morphology, and the reduction in podocyte slit pore density was not countered by the Smad3 KO, leading to the prediction that diabetic KO mice would remain albuminuric.

Despite the persistence of albuminuria in the diabetic KO mice, kidney function remained normal, as assessed by the plasma creatinine and the BUN. Nephroprotection in diabetes was also achieved with an anti-TGF-β treatment in *db/db* mice (23). In that study, kidney function was maintained, despite the persistent albuminuria (23), implying that albuminuria incites renal functional damage through the TGF-β system (14). Our present study goes one step further to suggest that the bulk of the harmful effects of TGF-β may be mediated by Smad3 signaling.

In summary, the Smad3 pathway plays a crucial role in the mechanisms whereby the overactivity of TGF-β gives rise to the structural manifestations of diabetic injury in the kidney. These include renal hypertrophy, GBM thickening, mesangial matrix expansion, and fibronectin overexpression. The prevention of these histopathological lesions may be sufficient to confer renoprotection, although the Smad3 KO may entail other beneficial effects. In contrast, the Smad3 pathway does not seem to participate in the process of diabetic albuminuria, which is probably more influenced by the VEGF system (5, 8, 20). Still, the effects of the Smad3 KO were closely matched with the historical benefits of anti-TGF-β therapy, arguing for a predominance of the Smad3 arm in mediating the injurious effects of TGF-β in diabetic kidney disease.

ACKNOWLEDGMENTS

The authors thank Evelyn Grau and Susan Pickering at GlaxoSmithKline for handling microinjections and animal husbandry. F. N. Ziyadeh and S. Chen are grateful to the University of Pennsylvania Renal Division where part of the work was done.

GRANTS

Research was supported by the National Institute of Diabetes and Digestive and Kidney Diseases (DK061537 to S. Chen and DK044513 to F. N. Ziyadeh), the American Heart Association (to F. N. Ziyadeh), a stipend from Ewha Womans University (to S. H. Sung), and an International Fellowship Award of the International Society of Nephrology (to E. Y. Lee).

REFERENCES

1. **Ashcroft GS, Yang X, Glick AB, Weinstein M, Letterio JL, Mizel DE, Anzano M, Greenwell-Wild T, Wahl SM, Deng C, Roberts AB.** Mice lacking Smad3 show accelerated wound healing and an impaired local inflammatory response. *Nat Cell Biol* 1: 260–266, 1999.
2. **Attisano L, Wrana JL.** Smads as transcriptional co-modulators. *Curr Opin Cell Biol* 12: 235–243, 2000.
3. **Benigni A, Zoja C, Corna D, Zatelli C, Conti S, Campana M, Gagliardini E, Rottoli D, Zanchi C, Abbate M, Ledbetter S, Remuzzi G.** Add-on anti-TGF-beta antibody to ACE inhibitor arrests progressive diabetic nephropathy in the rat. *J Am Soc Nephrol* 14: 1816–1824, 2003.
4. **Chen S, Iglesias-de la Cruz MC, Jim B, Hong SW, Isono M, Ziyadeh FN.** Reversibility of established diabetic glomerulopathy by anti-TGF-beta antibodies in *db/db* mice. *Biochem Biophys Res Commun* 300: 16–22, 2003.
5. **De Vriese AS, Tilton RG, Elger M, Stephan CC, Kriz W, Lameire NH.** Antibodies against vascular endothelial growth factor improve early renal dysfunction in experimental diabetes. *J Am Soc Nephrol* 12: 993–1000, 2001.
6. **Dunn SR, Qi Z, Bottinger EP, Breyer MD, Sharma K.** Utility of endogenous creatinine clearance as a measure of renal function in mice. *Kidney Int* 65: 1959–1967, 2004.
7. **Flanders KC.** Smad3 as a mediator of the fibrotic response. *Int J Exp Pathol* 85: 47–64, 2004.
8. **Flyvbjerg A, Dagnaes-Hansen F, De Vriese AS, Schrijvers BF, Tilton RG, Rasch R.** Amelioration of long-term renal changes in obese type 2 diabetic mice by a neutralizing vascular endothelial growth factor antibody. *Diabetes* 51: 3090–3094, 2002.
9. **Fujimoto M, Maezawa Y, Yokote K, Joh K, Kobayashi K, Kawamura H, Nishimura M, Roberts AB, Saito Y, Mori S.** Mice lacking Smad3 are protected against streptozotocin-induced diabetic glomerulopathy. *Biochem Biophys Res Commun* 305: 1002–1007, 2003.
10. **Isono M, Chen S, Hong SW, Iglesias-de la Cruz MC, Ziyadeh FN.** Smad pathway is activated in the diabetic mouse kidney and Smad3 mediates TGF-beta-induced fibronectin in mesangial cells. *Biochem Biophys Res Commun* 296: 1356–1365, 2002.
11. **Juarez P, Vilchis-Landeros MM, Ponce-Coria J, Mendoza V, Hernandez-Pando R, Bobadilla NA, Lopez-Casillas F.** Soluble betaglycan reduces renal damage progression in *db*/*db* mice. *Am J Physiol Renal Physiol* 292: F321–F329, 2007.
12. **Lahdenkari AT, Lounatmaa K, Patrakka J, Holmberg C, Wartiovaara J, Kestila M, Koskimies O, Jalanko H.** Podocytes are firmly attached to glomerular basement membrane in kidneys with heavy proteinuria. *J Am Soc Nephrol* 15: 2611–2618, 2004.
13. **Piek E, Ju WJ, Heyer J, Escalante-Alcalde D, Stewart CL, Weinstein M, Deng C, Kucherlapati R, Bottinger EP, Roberts AB.** Functional characterization of transforming growth factor beta signaling in Smad2- and Smad3-deficient fibroblasts. *J Biol Chem* 276: 19945–19953, 2001.
14. **Reeves WB, Andreoli TE.** Transforming growth factor beta contributes to progressive diabetic nephropathy. *Proc Natl Acad Sci USA* 97: 7667–7669, 2000.
15. **Roberts AB, Piek E, Bottinger EP, Ashcroft G, Mitchell JB, Flanders KC.** Is Smad3 a major player in signal transduction pathways leading to fibrogenesis? *Chest* 120: 43S–47S, 2001.
16. **Sato M, Muragaki Y, Saika S, Roberts AB, Ooshima A.** Targeted disruption of TGF-beta1/Smad3 signaling protects against renal tubulointerstitial fibrosis induced by unilateral ureteral obstruction. *J Clin Invest* 112: 1486–1494, 2003.
17. **Sharma K, Jin Y, Guo J, Ziyadeh FN.** Neutralization of TGF-beta by anti-TGF-beta antibody attenuates kidney hypertrophy and the enhanced extracellular matrix gene expression in STZ-induced diabetic mice. *Diabetes* 45: 522–530, 1996.
18. **Shi Y, Massague J.** Mechanisms of TGF-beta signaling from cell membrane to the nucleus. *Cell* 113: 685–700, 2003.
19. **Simon M, Gröne HJ, Jöhren O, Kullmer J, Plate KH, Risau W, Fuchs E.** Expression of vascular endothelial growth factor and its receptors in human renal ontogenesis and in adult kidney. *Am J Physiol Renal Fluid Electrolyte Physiol* 268: F240–F250, 1995.
20. **Sung SH, Ziyadeh FN, Wang A, Pyagay PE, Kanwar YS, Chen S.** Blockade of vascular endothelial growth factor signaling ameliorates diabetic albuminuria in mice. *J Am Soc Nephrol* 17: 3093–3104, 2006.
21. **Wu DT, Bitzer M, Ju W, Mundel P, Bottinger EP.** TGF-beta concentration specifies differential signaling profiles of growth arrest/differentiation and apoptosis in podocytes. *J Am Soc Nephrol* 16: 3211–3221, 2005.
22. **Yang X, Letterio JJ, Lechleider RJ, Chen L, Hayman R, Gu H, Roberts AB, Deng C.** Targeted disruption of SMAD3 results in impaired mucosal immunity and diminished T cell responsiveness to TGF-beta. *EMBO J* 18: 1280–1291, 1999.
23. **Ziyadeh FN, Hoffman BB, Han DC, Iglesias-de la Cruz MC, Hong SW, Isono M, Chen S, McGowan TA, Sharma K.** Long-term prevention of renal insufficiency, excess matrix gene expression, and glomerular mesangial matrix expansion by treatment with monoclonal antitransforming growth factor-beta antibody in *db/db* diabetic mice. *Proc Natl Acad Sci USA* 97: 8015–8020, 2000.